chemosensors

MDPI

Article

Ultrafast and Multiplexed Bacteriophage Susceptibility Testing by Surface Plasmon Resonance and Phase Imaging of Immobilized Phage Microarrays

Larry O'Connell [1,2], Ondrej Mandula [1], Loïc Leroy [2], Axelle Aubert [1], Pierre R. Marcoux [1,*] and Yoann Roupioz [2,*]

[1] Univ. Grenoble Alpes, CEA, LETI, F38054 Grenoble, France; oconnel1@tcd.ie (L.O.); ondrej.mandula@cea.fr (O.M.); axelle.aubert@cea.fr (A.A.)
[2] Univ. Grenoble Alpes, CNRS, CEA, IRIG, SyMMES, 38000 Grenoble, France; loic.leroy@univ-grenoble-alpes.fr
* Correspondence: pierre.marcoux@cea.fr (P.R.M.); yoann.roupioz@cea.fr (Y.R.); Tel.: +33-4-38-78-15-04 (P.R.M.); +33-4-38-78-98-79 (Y.R.)

Abstract: In the context of bacteriophage (phage) therapy, there is an urgent need for a method permitting multiplexed, parallel phage susceptibility testing (PST) prior to the formulation of personalized phage cocktails for administration to patients suffering from antimicrobial-resistant bacterial infections. Methods based on surface plasmon resonance imaging (SPRi) and phase imaging were demonstrated as candidates for very rapid (<2 h) PST in the broth phase. Biosensing layers composed of arrays of phages 44AHJD, P68, and gh-1 were covalently immobilized on the surface of an SPRi prism and exposed to liquid culture of either *Pseudomonas putida* or methicillin-resistant *Staphylococcus aureus* (i.e., either the phages' host or non-host bacteria). Monitoring of reflectivity reveals susceptibility of the challenge bacteria to the immobilized phage strains. Investigation of phase imaging of lytic replication of gh-1 demonstrates PST at the single-cell scale, without requiring phage immobilization. SPRi sensorgrams show that on-target regions increase in reflectivity more slowly, stabilizing later and to a lower level compared to off-target regions. Phage susceptibility can be revealed in as little as 30 min in both the SPRi and phase imaging methods.

Keywords: surface plasmon resonance imaging; phase imaging; phage susceptibility testing (PST); phage therapy; personalized cocktail; *Staphylococcus aureus*; phage microarray

Citation: O'Connell, L.; Mandula, O.; Leroy, L.; Aubert, A.; Marcoux, P.R.; Roupioz, Y. Ultrafast and Multiplexed Bacteriophage Susceptibility Testing by Surface Plasmon Resonance and Phase Imaging of Immobilized Phage Microarrays. *Chemosensors* **2022**, *10*, 192. https://doi.org/10.3390/chemosensors10050192

Academic Editors: Iole Venditti, Paolo Prosposito and Alessandra Paladini

Received: 22 April 2022
Accepted: 17 May 2022
Published: 19 May 2022

1. Introduction

1.1. Antimicrobial Resistance

The proliferation of multi-resistant bacteria is having an increasing and profound impact on health outcomes worldwide, with recent data reporting an overwhelming burden of 1.27 million deaths in 2019 attributable to bacterial antimicrobial resistance [1].

Within this context, alongside the possibility of discovery of novel classes of antimicrobials and stewardship of known molecules, phage therapy is enjoying increasing interest as a plausible alternative to classical antibiotics, which may in the near future form the basis of a new treatment paradigm for bacterial infections [2,3].

The host range of a phage depends on several factors but most strongly on its ability to specifically recognize and bind to cells of host bacterial strains via receptor-binding domains on the phage capsid [4]. Because of this specific binding, phages have a narrow host range that is species- or even strain-specific. This constrained spectrum of action presents an advantage in that an administered phage targeting a given pathogen need not disturb the normal commensal flora of the patient [5]. However, this narrow host range also presents challenges that must be mitigated, namely that screening must be performed to ascertain the susceptibility of a given bacterial pathogen to a range of candidate phages

in order to develop a cocktail personalized to each patient, composed only of phages to which the pathogen is susceptible.

Of the different morphologies and lifecycles exhibited by phages, only some are appropriate for phage therapy. Temperate phages must be avoided since lysogeny can confer virulence factors to the host bacteria via genetic transduction, increasing their pathogenicity [6]. Lytic phages are thus preferred since they are immediately lethal to their host bacteria and are less likely to enable horizontal gene transfer or induce superinfection immunity [2]. For these reasons, phages must be characterized and vetted on the above criteria (inter alia) before being incorporated into a library as suitable therapeutic agents [6].

1.2. Phage Susceptibility Testing

In order to facilitate a partial or wholesale transition from traditional antimicrobials to phage therapy, new tools are needed for rapid and multiplexed screening of large libraries of candidate phages in order to provide a personalized phage to each patient. Up to 100 different lytic phages may have to be screened to find active phages on the patient's bacterial isolate [7]. More typically, between 5 to 10 different phages are tested either in isolation or in various permutations as a cocktail, over a range of 5 to 9 concentrations, which places a requirement of high multiplexing capacity on any potential PST method.

Currently, the most frequently exploited methods for PST rely on phage–bacteria co-culture since, of the methods available, liquid culture lysis is the technique that appears to be the most easily extensible to scalable automation. Lysis culture assays can be carried out in industry-standard microdilution transfer plates [8], which can feature as few as six and as many as several hundred individual wells. This method also permits combinatorial assays to establish phage synergy or antagonism through a kind of pair-wise checkerboard assay [9]. Several works have demonstrated the use of plate readers adapted to monitor optical density of bacteria–phage co-culture [10–12].

However, these techniques rely on a spectrophotometric or colorimetric change that reveals phage replication with long time to results, ranging from 2 to 6 h [11,13]. Furthermore, to the authors' knowledge, there is no work yet describing the use of such methods for parallel comparison of phage–host affinity, as proposed in this work.

More recently, wide-field lens-free imaging has been leveraged to accelerate PST and even detect phage-resistant bacterial microcolonies with a time to results of only 3 h [14]. While such a method significantly reduces time to results, it has not yet been demonstrated in a scalable way that would be extensible to parallel screening of many phages within the same assay.

The aim of this work is to demonstrate a proof-of-concept parallel, multiplexed SPRi-based phage susceptibility screening assay. To this end, a biosensing layer featuring an array of different candidate phages is covalently immobilized on a gold surface and produces a measurable surface plasmon resonance signal correlated with interactions between immobilized phages and bacterial cells introduced to the sensor surface (Figure 1A). Monitoring of the interaction in real time of each of a large array of phages with a challenge bacterial strain would reveal those that are suitable for inclusion in a phage cocktail against that strain. In this sense, the envisaged assay would take the form of a single-use SPRi consumable, in analogy to convenience of commercially available antibiotic susceptibility systems.

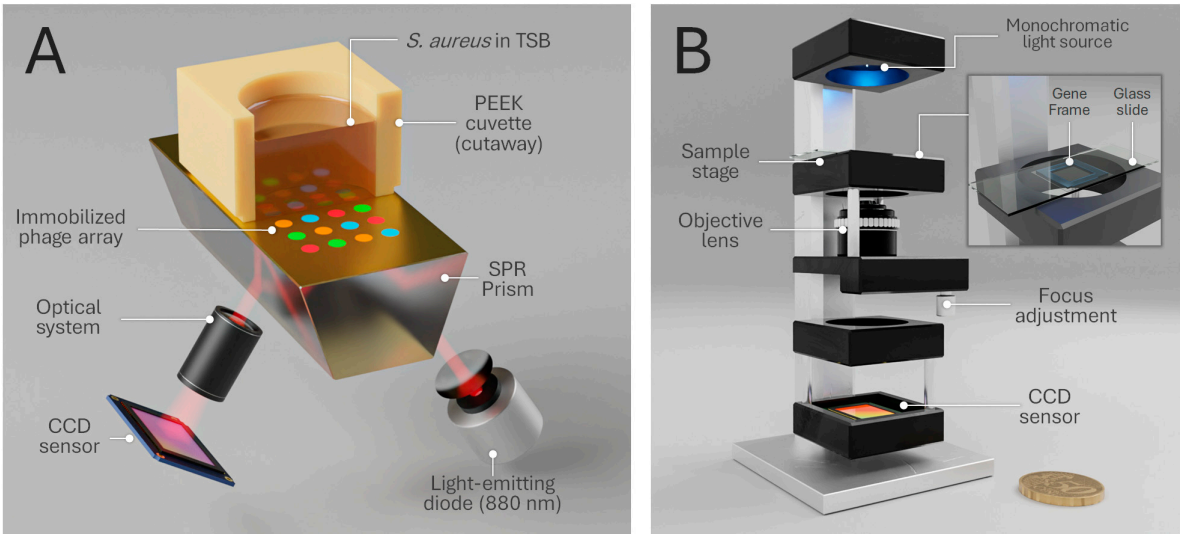

Figure 1. (**A**) A schematic illustration of the SPRi prism, functionalized with an immobilized array of phages, shown interfaced with a cutaway of the PEEK cuvette containing liquid cultures of the challenge strain *Staphylococcus aureus*. (**B**) A schematic illustration of the phase imaging microscope. Mounted on the sample stage is a co-culture of phage gh-1 and *P. putida*, sandwiched between a microscope cover slip, a gas-impermeable Gene Frame, and a microscope slide.

1.3. Surface Plasmon Resonance

Surface plasmon resonance sensing relies on the coupling of light to surface plasmons and allows the transduction of physical binding phenomena on the sensor surface into an optical signal. A key strength of SPR is its high sensitivity to changes in the refractive index within the ~100 nm penetration depth of the sensor surface and exclusion of contributions beyond this region, allowing even small mass uptake of 10–0.01 pg/mm^2 of proteinous material to yield a measurable signal [15].

Surface plasmon resonance imaging (SPRi) builds on the strength of SPR by imaging the entire surface of a sensor (1–2 cm^2) that can be functionalized with many different ligands, simultaneously monitoring the interaction of each functionalized region in a single, parallel, multiplexed assay [16,17]. SPRi has been demonstrated for the specific detection—and potentially even identification and typing—of challenge bacteria using arrays of immobilized antimicrobial proteins [18]. In contrast to state-of-the-art PST methods involving optical measurements of bacteria/phage co-culture in multiwell plates, SPRi arrays can feature many hundreds to thousands of probes arrayed on a single sensor surface.

To the authors' knowledge, this work represents the first time SPRi has been exploited for PST. A 2019 review of phage isolation and characterization techniques made no mention of SPR-based methods of PST [19], and the authors are aware of no such precedent in the literature.

The use of surface plasmon resonance for PST necessitates the localized, addressable immobilization of phages on the sensor surface, a task which is far from trivial [20,21]. We thus tested an alternative optical PST method, in parallel with SPR experiments, based on label-free digital holography.

1.4. Phase Imaging

Optical label-free techniques have been demonstrated to be effective for non-destructive characterization of bacterial pathogens, phenotypic identification [22] and viability assays [23], not only at the level of colonies [24] and microcolonies [25], but also down to the scale of single-cells [26]. In particular, imaging of phage plaques with wide-field lens-less techniques was recently reported to enable rapid solid-phase phage susceptibility testing with time to results as low as 4h20 for anti-*Staphylococcus aureus* phage and 2h20 for anti-*Klebsiella pneumoniae* phage [14]. In this case, a wide field-of-view (FoV) of 3.3 cm^2

was necessary to observe a sufficient number of lysis plaques. Considering instead PST in the broth phase, it may be advantageous to sacrifice FoV to gain resolution, with a view to imaging single cells, counting them directly, and even visualizing individual lysis events. For this reason, phase imaging experiments were performed with phage gh-1 and its host *P. putida*, in parallel with surface plasmon resonance experiments, to investigate bacterium–phage interaction at the single-cell scale. Phase imaging techniques, such as Zernike phase contrast, differential interference contrast, or digital holography microscopy, allow observation of non-absorbing or poorly absorbing objects such as individual cells immersed in nutritive medium. Bringing the sample slightly out of focus creates well-contrasted interference fringes in the image plane that emphasizes cells but degrades image quality due to diffraction. Post-acquisition analysis of images allows one to recover accurate imagery of bacterial cells and carry out precise monitoring of biomass over the entire FoV.

2. Materials and Methods

2.1. Materials

Glycerol (≥99%), 11-mercaptoundecanoic acid (11-MUA, 95%), agar (Difco), bovine serum albumin (BSA), ethanolamine (≥99.5%), trypticase soy broth (TSB), potassium nitrate (KNO_3), and ethanol (≥99.9%) were purchased from Sigma-Aldrich (Saint Quentin Fallavier, France) and used without additional purification. CsCl (≥99.9%), 0.9% *w*/*v* NaCl solution (OTEC), and 90 mm tryptone soy agar (TSA) Petri plates were purchased from VWR (France). 1-Ethyl-3-(3-dimethylaminopropyl)carbodiimide (EDC) (≥98%) and sulfo-N-Hydroxysuccinimide (sulfo-NHS) were purchased from Thermofisher and used as received. Deionized water (DIW; >18 MΩ resistivity) was obtained from an ELGA PURELAB flex dispenser (Veolia Water, France). Polyethylene glycol 6 kDa (PEG-6000) was purchased from Merck (Darmstadt, Germany).

2.2. Host Bacterium and Bacteriophage Preparation

Bacterial host *Pseudomonas putida* (ATCC 12633; host of phage gh-1) and phages 44AHJD [27], P68, and gh-1 [28] were obtained from the Félix d'Hérelle Reference Center for Bacterial Viruses of Université Laval, Quebec, Canada. Bacterial hosts *Staphylococcus aureus* subsp. *aureus* Rosenbach (SA1; ATCC 43300, host of phage 44AHJD@SA1) and *Staphylococcus aureus* (SA2; ATCC BAA-2312, host of phages 44AHJD@SA2 and P68@SA2) were obtained from Microbiologics (Kwik-Stik^{TM} lyophilized strain).

Bacterial cultures were routinely prepared in TSB at recommended temperatures for each host: *S. aureus* at 37 °C and *P. putida* at 30 °C. Phage suspensions were routinely prepared using the double-layer agar method [29]: 100 µL of overnight liquid precultures of each bacterial host were inoculated into fresh TSB and allowed to proliferate until reaching 10^8 colony-forming units per mL (CFU/mL) as confirmed by optical density at 550 nm. Then, 200 µL bacterial host and 100 µL phage suspension were inoculated into each of several 15 mL Falcon tubes filled with 5 mL molten agar (TSB prepared with 7.5 g/L agar) at 51.5 °C, vortexed, and poured over 20 mL solidified tryptic soy agar (TSA, 15 g/L agar) in a standard 90 mm Petri plate. Plates were then incubated overnight until lysis plaques became confluent in the top agar layer, which was then collected and soaked for 4 h at room temperature in sterile 154 mmol NaCl solution in a 50 mL polypropylene tube. Each tube was then twice centrifuged for 20 min 5500× *g* at 4 °C, and the supernatant was retained each time.

Rigorous purification of phage suspensions is an essential step and was achieved using a combination of PEG/NaCl precipitation, ultracentrifugation, and ultrafiltration. Each suspension (35–45 mL) was brought to 0.5 mol NaCl and 8% *w*/*v* PEG-6000 and left at 4 °C overnight to precipitate the phages. The following day, each suspension was centrifuged for 30 min at 12,000× *g* at 4 °C, the supernatant removed, and the pellet resuspended in sterile 154 mmol NaCl, vortexed, centrifuged 20 min 5500× *g* at 4 °C and the supernatant was retained.

Suspensions were then further purified by density gradient ultracentrifugation for 2 h at 100,000× *g* at 4 °C on a CsCl step gradient (1.7 g/mL, 1.54 g/mL, and 1.34 g/mL CsCl in DIW) in 5 mL, Open-Top Thinwall Ultra-Clear ultracentrifuge tubes (Beckman Coulter, Villepinte, France) in a SW55Ti swinging-bucket rotor (Beckman Coulter) mounted in an Optima l-90K Ultracentrifuge (Beckman Coulter). Phages were concentrated at the second visible band from the top and collected with a micropipette. Finally, CsCl and small-molecular-weight contaminants were then removed from phage suspensions by twice repeated centrifugal ultrafiltration and resuspension in 154 mmol NaCl solution using 100 kDa Vivaspin 500 ultrafiltration units (Sartorius).

All phage suspensions were stored at 4 °C in the dark in 1.5 mL polypropylene Eppendorf-type tubes. Following purification, the infectious titer of phage suspensions was obtained by the agar overlay method [29] and is reported in units of plaque-forming units per milliliter (PFU/mL). Phages capable of using several bacterial strains as their hosts are appended with the abbreviation of the host used—44AHJD amplified with SA1 is referred to as 44AHJD@SA1, while 44AHJD amplified with SA2 is referred to as 44AHJD@SA2, etc.

2.3. Substrate Preparation

Gold-coated SPR prisms were purchased from Horiba (SPRi-Biochips™, Horiba Scientific, Palaiseau, France). The gold surface of the prism was rinsed with DIW, ultrapure ethanol, then once more with DIW. The prism was then dried with argon and plasma cleaned for 3 min in 0.6 mBar 75:25 oxygen/argon mix at 80% power in a Femto plasma system (Diener electronic, Ebhausen, Germany). The prism surface was then left at room temperature to stabilize for at least 24 h before use.

2.4. Bacteriophage Immobilization

11-MUA was dissolved in ultrapure ethanol to a concentration of 50 mmol. The cleaned gold surfaces of SPR prisms were functionalized with 11-MUA to form a self-assembled monolayer (SAM) by soaking the entire SPR prism overnight at room temperature. Before phage immobilization, the prisms were rinsed with ultrapure ethanol, dried with compressed air, and submerged in a 100 mmol EDC, 25 mmol sulfo-NHS aqueous solution for 30 min at room temperature to activate the carboxyl groups of the 11-MUA SAM. The surface was then rinsed with DIW, dried with compressed air, and immediately deposited with phage suspensions—154 mmol NaCl supplemented with 10% *w*/*v* glycerol with an infectious titer of 6×10^9 PFU/mL for P68 and 10^{11} PFU/mL for other phages. Addition of glycerol has been found to be a crucial step to prevent drying of small deposited droplets, permitting the arrayed immobilization of different phage species in adjacent, closely-spaced regions on the same substrate [20].

In this work, SPR prisms were spotted either manually or using a microarrayer deposition system. Robot-assisted spotting was carried out using a method described elsewhere [20]. Briefly, the prism is mounted in an automated microarrayer system (OmniGrid Micro, Genomic Solutions Inc., Irvine, CA, USA) fitted with a 350 µm-diameter stylus (Xtend, LabNEXT Inc., West New York, NY, USA). A total of 100 µL of each phage suspension was loaded in a standard PCR tube, retrieved by the stylus, and a volume of approximately 10 nL was deposited on the prism surface, producing circular phage-functionalized regions 500–600 µm in diameter. For manually spotted prisms, a micropipette was used to drop cast 1 µL droplets of each phage suspension on the prism surface.

For both deposition methods, phage suspensions were incubated with the surface overnight at room temperature in a humid environment inside a chamber loaded with saturated KNO_3 solution (95% relative humidity) and rinsed with DIW the following day. Before the surface plasmon resonance imaging, the prism was immersed in 100 mmol ethanolamine aqueous solution for 30 min followed by 1 mg/mL BSA aqueous solution for 10 min in order to block the surface against non-specific binding, then rinsed thoroughly with DIW. The prism surfaces were at no point allowed to dry once phages had been immobilized, since this is known to inactivate many species of phage [30,31].

2.5. Phage–Bacteria Interaction Monitoring by Surface Plasmon Resonance Imaging

The monitoring of immobilized phage interactions with bacteria was performed using a commercial SPRi device (SPRiLab, Horiba Scientific, Orsay, France) placed in an incubator at either 33.5 °C or 37 °C depending on the experiment. The SPRi prism was interfaced to a PEEK cuvette, which permitted the introduction of an analyte to the sensor surface (Figure 1A). The cuvette was filled with sterile TSB and plasmon curves recorded for all functionalized regions of the sensor surface. The cuvette opening was covered with labfilm to prevent evaporative concentration of the analyte.

Exponential-phase cultures of *P. putida* and *S. aureus* in TSB were pelleted by centrifugation at 5500× *g* at room temperature for 5 min, resuspended in fresh TSB, centrifuged and resuspended a second time in TSB to a concentration of either 10^6 or 10^9 CFU/mL, and then a volume of 1 mL was introduced to the sensor surface with one strain in each chamber. Reflectivity shifts were then recorded, with images taken every six seconds.

2.6. Phase Imaging

We used a custom phase imaging microscope setup (Figure 1B) in an inverted configuration that has been described elsewhere in the work of Mandula et al. [32]. Briefly, a bright field of 20×, 0.4 numerical aperture, infinity-corrected, dry objective (Motic) with f = 50 mm tube lens creates a magnified image of the sample on a CMOS chip (IDS UI-1490SE-M-GL). A blue LED (450 nm, CREE) coupled to a multi-mode fiber (400 µm diameter, Thorlabs) placed at 5 cm above the sample provides a semi-coherent illumination in transmission geometry.

A chamber was made by sandwiching a Gene Frame (1 cm × 1 cm, 250 µm thick, Thermofisher) between a standard microscope slide and cover slip, forming a volume of 25 µL (Figure 1B). A co-culture of phage gh-1 and *P. putida* was mixed (10^8 phage/mL and 10^7 bacteria/mL), and 20 µL was immediately introduced into the Gene Frame chamber.

The slide and chamber were placed on the sample stage and inverted with the coverslip facing the objective. The inner surface of the coverslip covered with sedimented bacteria was deliberately placed ~5 µm out of focus to create better contrast between bacteria and the background. A time-lapse was recorded over 80 min at 30 s intervals (see Supplementary Video S1 of the corresponding ROI).

2.7. Data Analysis

SPRi reflectivity data were captured using SPRiView (v3.1.2) and processed using MatLab R2021a (v9.10). Regions of interest (ROIs) were manually selected during initialization of the SPRi experiment, chosen to correspond to the phage-functionalized regions of the surface. The reflectivity signal was averaged across the area of each ROI. A one-minute rolling average (i.e., mean of 20 data points) was then taken of the resultant traces. No blank subtraction or drift correction was necessary to reveal the phage–host interactions.

In phase imaging experiments, time-lapse imagery was processed to detect individual bacteria using Laplace of Gaussian detection with an estimated blob diameter of 3 µm, using ImageJ plugin TrackMate [33]. Supplementary Video S2 shows bacterial cell detection within the phase-imaging ROI.

3. Results

3.1. SPR

In order to investigate interactions between sensor surfaces and challenge bacterial strains, phages were immobilized in a 10 × 6 rectilinear array using a microarrayer system [20], and the array was exposed to TSB containing methicillin-resistant *S. aureus* (SA1, host of 44AHJD@SA1) to demonstrate susceptibility screening of a clinically relevant pathogen (i.e., a member of the ESKAPE group of pathogens [34]). A moderate concentration of bacteria of 10^6 CFU/mL was introduced to the surface to represent a reasonable concentration of analyte comparable to that likely to be available in a clinical setting.

In order to compare the response of several phages with varying levels of affinity to the challenge strain, four candidate phages were immobilized in separate regions: an *off-target* phage gh-1, which is incapable of replicating with SA1 as its host, an *on-target* phage 44AHJD@SA1, which is capable of replicating with SA1, and two additional candidate phages—P68@SA2 and 44AHJD@SA2—which had both been amplified with a different species of *S. aureus* (SA2; ATCC BAA-2312) than the challenge strain SA1. The purpose of including P68@SA2 and 44AHJD@SA2 is that we may expect them to have an intermediate affinity for the challenge bacteria, between that of gh-1 and 44AHJD@SA1, due to evolutionary pressure on receptor-binding domains during phage amplification.

The results of previous experiments indicate that the purification and immobilization protocol used in this work consistently yields homogenous, high-purity, high-density (90–160 phage/μm^2) phage monolayers from suspensions of phages gh-1 and 44AHJD (unpublished results). This arraying method allows several replicates of each phage to be immobilized on the surface and demonstrates the extensibility of the proposed technique to arrays of many dozens or hundreds of phages.

Plotting the reflectivity shifts revealed that the reflectivity of on-target regions (i.e., regions where a phage is exposed to its host) increased most slowly and stabilized to a lower value (Figure 2, dashed orange line) compared to off-target (black line) and intermediate regions (solid orange and blue lines). Interestingly, the sensorgram revealed a spread of responses, which reflects the expected affinity of each phage for the challenge bacteria. While 44AHJD@SA1 exhibited the strongest response (slowest reflectivity increase), 44AHJD@SA2 showed the next strongest response, which correlates well with its reduced (but non-zero) ability to use this bacterial strain as a host. Continuing the pattern, P68@SA2 is another phage that uses a related *S. aureus* strain as its host and exhibited the next strongest response after 44AHJD@SA2. Phages 44AHJD@SA2 and P68@SA2 are the product of several rounds of amplification on SA2; it may be that these immobilized phages exhibit an increased affinity for the SA2 strain as a result of selective pressure on the host-determining regions of the phage receptor-binding domains.

Finally, phage gh-1 is entirely incapable of replicating on the challenge strain, and we observed the weakest response from this phage. Nevertheless, we see an increase in reflectivity in these regions. We attributed this to the increase in concentration of bacteria in the cuvette above the off-target regions as bacteria sedimented across the entire sensor surface as the experiment progresses.

Considering the first derivatives of the sensorgrams (Supplementary Figure S1), we observed that on-target regions peaked with a lower rate of change in reflectivity compared to all other regions. Despite the difference in peak rate of change, the first derivatives of sensorgram traces of both on and off-target regions all peaked within 25 min of one another.

In order to validate the above result through cross-comparison of phage interactions with two separate bacterial hosts, phages were again immobilized, this time in duplicate arrays on the sensor surface, with each duplicate array exposed to one of two chambers containing TSB inoculated with either *P. putida* (host of gh-1) or *S. aureus* (SA1, host of 44AHJD@SA1).

Again, we observed the same effect where the reflectivity levels of on-target regions increased most slowly and stabilized to a lower value compared to off-target regions (Figure 3). This effect is especially clear in the first derivative of the reflectivity (Supplementary Figure S2), where the signals of off-target regions increase immediately in response to the introduction of bacteria and reach a higher peak (at 25 and 29 min for gh-1 + *S. aureus* and 44AHJD@SA1 + *P. putida*, respectively), while on-target regions lag behind and reach a lower peak value and do so later (at 119 and 86 min for gh-1 + *P. putida* and 44AHJD@SA1 + *S. aureus*, respectively) compared to the first derivative of off-target regions. The specific response of phages to their host is revealed within in the first 30 min after introduction of bacteria at a high concentration of 10^9 CFU/mL.

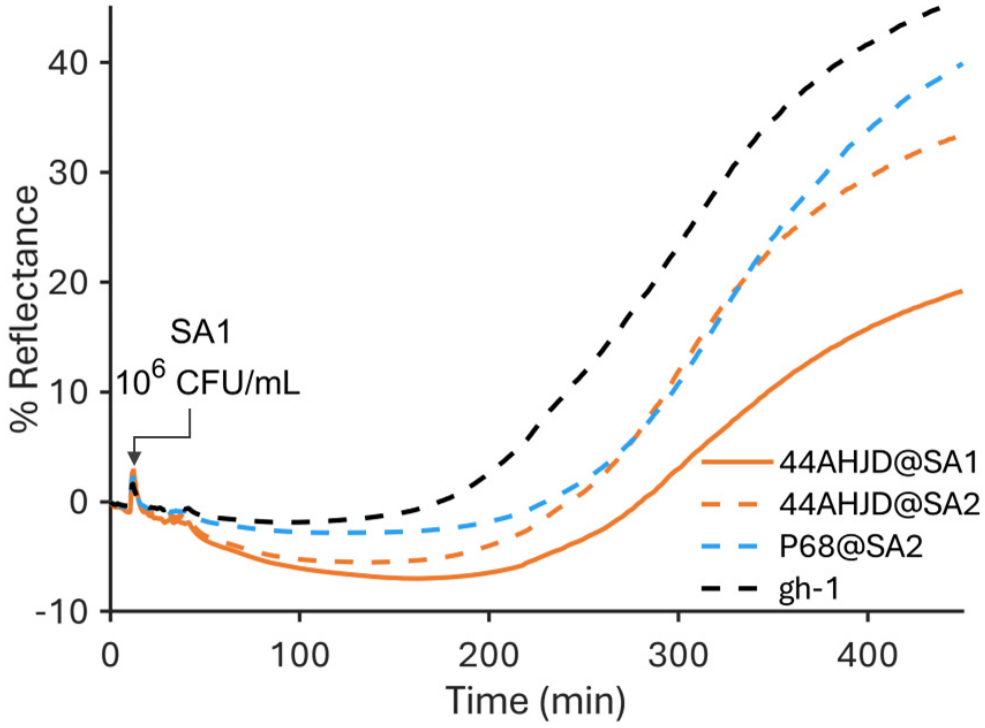

Figure 2. Sensorgram showing the SPR responses of regions functionalized with phages 44AHJD@SA1 (solid orange lines), 44AHJD@SA2 (dashed orange lines), P68@SA2 (blue lines) and gh-1 (black lines) when exposed to *S. aureus* SA1. Traces show a one-minute rolling average (i.e., mean of 20 data points).

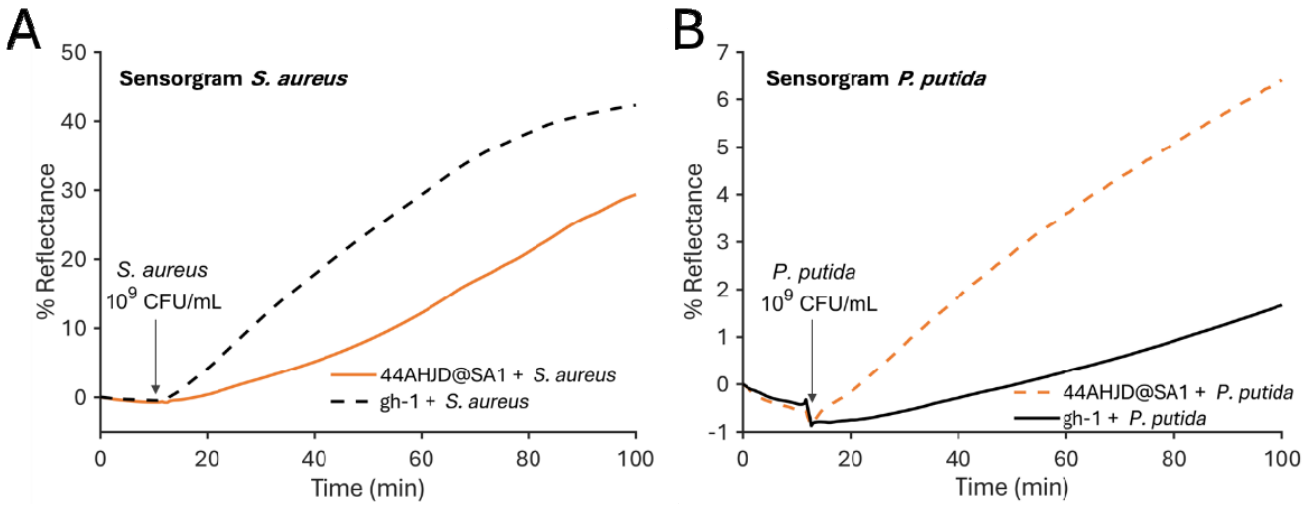

Figure 3. Sensorgrams showing the SPR responses of regions functionalized with phages 44AHJD@SA1 (orange lines) and gh-1 (black lines) when exposed to *S. aureus* (**A**) or *P. putida* (**B**). Traces show a one-minute rolling average (i.e., mean of 20 data points).

In addition, the response time of the sensor was shortened relative to the previous experiment, with the inflection points of off-target sensorgram traces occurring at 26 min for gh-1 exposed to S. aureus and 29 min for 44AHJD@SA1 exposed to *P. putida*, approximately 10 times faster than in the first experiment after injection of SA1 where all curves peaked around 315 ±10 min. We attribute this faster result to the much higher concentration of bacteria in the second experiment of 10^9 CFU/mL, compared to 10^6 CFU/mL in the first.

While *P. putida* is a motile bacterium [35], *S. aureus*—barring special circumstances—is non-motile [36]. For this reason, the sedimentation of *S. aureus* onto the sensor surface is

likely to progress more rapidly than for *P. putida*, having the effect of facilitating increased interaction between *S. aureus* and the sensor surface. This may account for the more rapid development of reflectivity under the *S. aureus* chamber in this experiment.

Since this second type of experiment exposed identically phage-functionalized regions to two different challenge strains during the same experiment, the relative SPR responses of each phage are directly comparable. Several potential sources of experimental variability are controlled for in this two-chamber setup. Firstly, any variation in the upstream processing of the substrate (e.g., cleaning, chemical activation, etc.) is controlled for since all phages are immobilized on the same surface. Phage titer can be unstable in aqueous suspensions, which brings the risk that otherwise identical substrates prepared on different days may be incubated with phage suspensions with different aggregation states and/or infectious titers [37,38]. Any differences in the phage response between the two chambers can reliably be considered to originate in the divergent response of each phage to each challenge strain, providing strong preliminary support for the feasibility of the proposed method of susceptibility testing.

The phage–host pairs in this work were chosen to include bacteria-featuring membranes with very different characteristics. While *S. aureus* is Gram-positive, *P. putida* is Gram-negative, and so the two types of cells differ significantly in cell wall composition. The receptor of phage gh-1 is known to be lipopolysaccharide [39], which is present in *P. putida* but absent in the Gram-negative *S. aureus*.

In contrast, podoviridae infecting *S. aureus* are known to require the presence of teichoic acid in the bacterial surface in order to absorb to their host [40]. Teichoic acid is present in the cell wall of *S. aureus* but absent in that of Gram-negative *P. putida*. For these reasons, we consider it to be a reasonable conclusion that the observed lack of activity in off-target phage/host pairs is well correlated with an inability of phages to bind to cells of the off-target bacterial strain.

3.2. Phase Imaging

In order to explore PST at the scale of single cells, phase imaging experiments were performed to observe bacterial lysis due to phage replication, over a population of several thousand cells within the FoV (Figure 4A). Computational reconstruction was carried out to permit imaging of scattering centers (i.e., bacteria) 200 µm below the observation plane, coinciding with the lower surface of the Gene Frame chamber, on the glass cover slip. Figure 4C shows the number of detected bacteria over time, when gh-1 phages are present, on the upper glass surface (red curve, observation plane) and on the lower glass surface (green curve, reconstructed image). For the first 35 min, the number of detected bacteria is observed to increase due to exponential division (Figure 4B), reaching a peak after 35 min. The increase is slightly larger on the lower surface (red curve) as the lower glass slide collects bacteria that sediment. A shallow decrease is followed by a steep drop at 39 min with the fastest decrease at 43 min. In a 20 min interval from 35 min to 100 min, the number of bacteria drops by 94%, coinciding with widespread phage-induced lysis (see Supplementary Video S2). Larger, out-of-focus features in the background of these images are due to motile bacteria outside of the focal plane of the microscope. In the control experiment without phages, similar curves are shown in Figure 4D, plotting biomasses on the upper and lower surfaces: they both reveal a continuous increase throughout the experiment. Once again, the increase in biomass is slightly larger for the red curve corresponding to the lower surface because of the sedimentation of bacteria.

Interestingly, bacteria can be observed to continue growing and dividing up until lysis (Supplementary Video S1), indicating that the cellular metabolism is not entirely diverted toward phage synthesis.

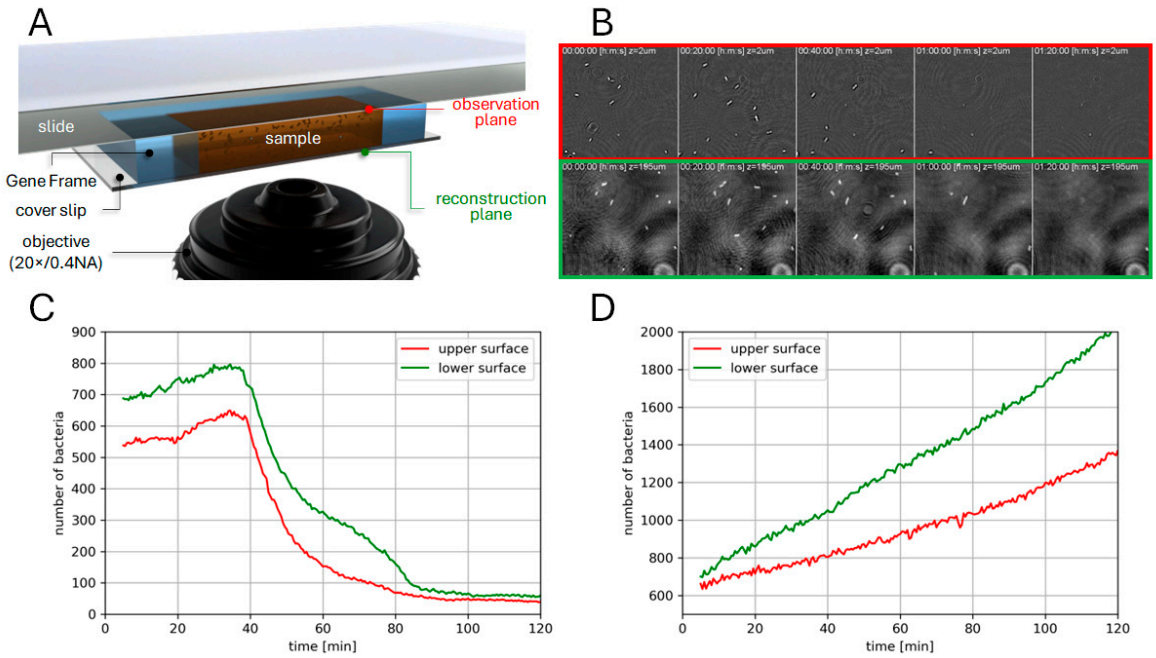

Figure 4. (**A**) Schematic of the optical setup for phase imaging of phage–bacteria interactions. The position of the glass slide was adjusted such that its upper surface was coincident with the observation plane. Images can be reconstructed in any plane within the volume enclosed by the Gene Frame, e.g., on the surface of the lower glass slide. Not to scale. (**B**) A sequence of 100 µm × 100 µm regions of interest extracted from the time-lapse of the observation plane (top row) and in the reconstructed image in the plane of the lower surface (bottom row). (**C**) Total number of bacteria vs. time in presence of gh-1 bacteriophages on the observation plane (red) and on the reconstructed plane (green). (**D**) Total number of bacteria vs. time (negative control without phages) on the observation plane (red) and on the reconstructed plane (green).

While the large FoV brought by our system enables the continuous monitoring of thousands of cells (Figure 5B), a thorough investigation of a given cell as a function time reveals that the phage-induced lysis follows a three-step process (Figure 5A). First, the degradation of peptidoglycan through endolysins is not visible, until the infected cell loses its bacillus shape and becomes a spheroplast [41,42]. At this stage, the outer and inner membrane still exist and take a round shape due to osmotic pressure. In the final stage of the lytic process, membranes disappear. Interestingly, phase imaging allows sufficient contrast to allow the observation of the bacterial debris that remains on the glass surface following phage lysis.

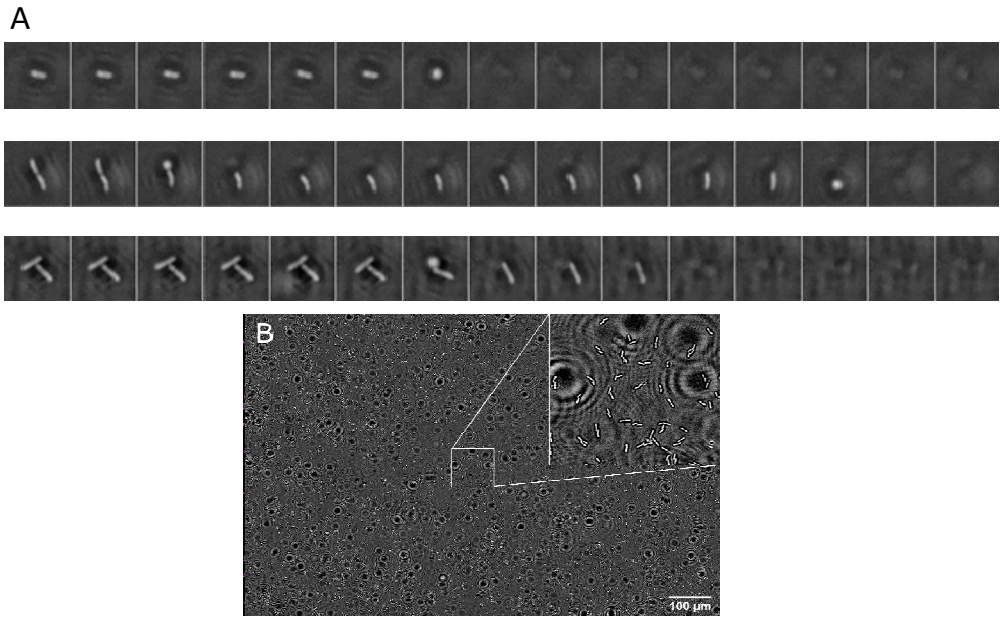

Figure 5. (**A**) Time-lapse sequences in three regions of interest, illustrating the different phases of lysis resulting from phage replication. (**B**) The entire FoV of our system (1.1 mm × 0.8 mm) with bacteria observed on the inner surface of the coverslip (bright rods) covering the gene frame chamber. Inset shows a magnified region of interest of 100 µm × 100 µm.

4. Discussion

A 2014 report by the World Health Organization [43] makes it increasingly clear that we must decrease our reliance on profligate and prophylactic administration of antibiotics in order to limit the proliferation of antimicrobial resistance genes. In order to enable new treatment paradigms in the context of healthcare and agribusiness, novel methods such as SPRi and phase-imaging PST may prove to be indispensable tools.

This work demonstrates a proof-of-concept SPRi-based method of rapid, multiplexed phage susceptibility testing. Specific responses of immobilized phages to their host are revealed as a lag in reflectivity increase. High concentrations of analyte bacteria (10^9 CFU/mL) can yield results within 30 min compared to several hours with state-of-the-art susceptibility testing methods.

Phage microarraying allows addressable immobilization of an array of dozens up to hundreds of different phage strains on the same surface [20]. Array pitch of 800 µm is consistently achievable with this technique, potentially permitting as many as 400 spots on the ~290 mm^2 surface area available on prisms used in this work, even before further refinement of the deposition parameters.

While covalent immobilization of phages via thiolated SAMs is a popular method [21], phage stability in this conjugated state is still an unknown. The challenge of variable phage stability may impact the interpretability of SPR sensorgram curves since differences in sensor response may originate in differences in the quality and density of the immobilized phage layer rather than differences in phage affinity. In this experiment, phages were immobilized within 24 h before use in SPRi experiments. Stability experiments are required to establish the reproducibility of SPRi-based PST with a larger variety of substrate-immobilized phages, and if the method presented in this work is compatible with long-term storage of the functionalized prism.

An alternative to SPRi PST was investigated in the form of phase imaging of phage-induced bacterial lysis. This method allows us to observe bacterial susceptibility within a physically compact region with a surprisingly simple apparatus and without the need for labelling bacteria or covalent immobilization of phage on a sensor surface.

Further development of SPRi and phase-imaging-based PST is needed to scale up throughput to screening of hundreds of candidate phage strains.

Supplementary Materials: The following supporting information can be downloaded at: https://www.mdpi.com/article/10.3390/chemosensors10050192/s1, Figure S1: First derivatives of SPR responses of regions exposed to *S. aureus* SA1.; Figure S2: First derivatives of SPR responses of regions exposed to *S. aureus* and *P. putida*.; Video S1: Phase Imaging Region of Interest; Video S2: Phase Imaging Cell Detection.

Author Contributions: Conceptualization, P.R.M. and Y.R.; formal analysis, L.O., O.M., A.A. and L.L.; funding acquisition, P.R.M. and Y.R.; resources, O.M., P.R.M. and Y.R.; software, L.O. and O.M.; supervision, P.R.M. and Y.R.; validation, P.R.M. and Y.R.; visualization, L.O., A.A. and O.M.; writing—original draft preparation, L.O. and O.M.; writing—review and editing, P.R.M. and Y.R. All authors have read and agreed to the published version of the manuscript.

Funding: This work has been partially supported by Labex ARCANE and CBH-EUR-GS (Grant ANR-17-EURE-0003).

Institutional Review Board Statement: Not applicable.

Informed Consent Statement: Not applicable.

Data Availability Statement: The data presented in this study are available on request from the corresponding authors.

Acknowledgments: The Félix d'Hérelle Reference Center for Bacterial Viruses at the Université Laval (Québec, Canada) is gratefully acknowledged for providing bacteriophages 44AHJD, P68 and gh-1, as well as bacterial host strain *Pseudomonas putida* (ATCC 12633). All image credits are to the authors unless otherwise stated. The authors would like to acknowledge the contribution of the Blender project, without which the illustrations in this work would not have been possible.

Conflicts of Interest: The authors declare no conflict of interest.

References

1. Murray, C.J.L.; Ikuta, K.S.; Sharara, F.; Swetschinski, L.; Aguilar, G.R.; Gray, A.; Han, C.; Bisignano, C.; Rao, P.; Wool, E.; et al. Global Burden of Bacterial Antimicrobial Resistance in 2019: A Systematic Analysis. *Lancet* **2022**, *399*, 629–655. [CrossRef]
2. Kakasis, A.; Panitsa, G. Bacteriophage Therapy as an Alternative Treatment for Human Infections. A Comprehensive Review. *Int. J. Antimicrob. Agents* **2019**, *53*, 16–21. [CrossRef] [PubMed]
3. Jault, P.; Leclerc, T.; Jennes, S.; Pirnay, J.P.; Que, Y.; Resch, G.; Rousseau, A.F.; Ravat, F.; Carsin, H. Efficacy and Tolerability of a Cocktail of Bacteriophages to Treat Burn Wounds Infected by Pseudomonas Aeruginosa (PhagoBurn): A Randomised, Controlled, Double-Blind Phase 1/2 Trial. *Lancet Infect. Dis.* **2018**, *3099*, 1–11. [CrossRef]
4. Hyman, P.; Abedon, S.T. *Bacteriophage Host Range and Bacterial Resistance*, 1st ed.; Elsevier Inc.: Philadelphia, PA, USA, 2010; Volume 70.
5. Loc-Carrillo, C.; Abedon, S.T. Pros and Cons of Phage Therapy. *Bacteriophage* **2011**, *1*, 111–114. [CrossRef] [PubMed]
6. Gill, J.; Hyman, P. Phage Choice, Isolation, and Preparation for Phage Therapy. *Curr. Pharm. Biotechnol.* **2010**, *11*, 2–14. [CrossRef] [PubMed]
7. Ferry, T.; Kolenda, C.; Resch, G. *Personalized Bacteriophage Therapy to Treat Pandrug-Resistant Spinal P. Aeruginosa Infection*; pp. 1–7. Available online: https://www.researchsquare.com/article/rs-1231457/v1 (accessed on 15 April 2022).
8. Dougherty, P.F.; Yotter, D.W.; Matthews, T.R. Microdilution Transfer Plate Technique for Determining in Vitro Synergy of Antimicrobial Agents. *Antimicrob. Agents Chemother.* **1977**, *11*, 225–228. [CrossRef]
9. Agún, S.; Fernández, L.; González-Menéndez, E.; Martínez, B.; Rodríguez, A.; García, P. Study of the Interactions between Bacteriophage PhiIPLA-RODI and Four Chemical Disinfectants for the Elimination of Staphylococcus Aureus Contamination. *Viruses* **2018**, *10*, 103. [CrossRef]
10. Cooper, C.J.; Denyer, S.P.; Maillard, J.Y. Rapid and Quantitative Automated Measurement of Bacteriophage Activity against Cystic Fibrosis Isolates of Pseudomonas Aeruginosa. *J. Appl. Microbiol.* **2011**, *110*, 631–640. [CrossRef]
11. Henry, M.; Biswas, B.; Vincent, L.; Mokashi, V.; Schuch, R.; Bishop-Lilly, K.A.; Sozhamannan, S. Development of a High Throughput Assay for Indirectly Measuring Phage Growth Using the OmniLog TM System. *Bacteriophage* **2012**, *2*, 159–167. [CrossRef]
12. Estrella, L.A.; Quinones, J.; Henry, M.; Hannah, R.M.; Pope, R.K.; Hamilton, T.; Teneza-mora, N.; Hall, E.; Biswajit, B. Characterization of Novel Staphylococcus Aureus Lytic Phage and Defining Their Combinatorial Virulence Using the OmniLog® System. *Bacteriophage* **2016**, *6*, e1219440. [CrossRef]
13. Rajnovic, D.; Muñoz-Berbel, X.; Mas, J. Fast Phage Detection and Quantification: An Optical Density-Based Approach. *PLoS ONE* **2019**, *14*, 1–14. [CrossRef] [PubMed]

14. Perlemoine, P.; Marcoux, P.R.; Picard, E.; Hadji, E.; Zelsmann, M.; Mugnier, G.; Marchet, A.; Resch, G.; O'Connell, L.; Lacot, E. Phage Susceptibility Testing and Infectious Titer Determination through Wide-Field Lensless Monitoring of Phage Plaque Growth. *PLoS ONE* **2021**, *16*, 1–14. [CrossRef] [PubMed]
15. Schasfoort, R.B.M. *Handbook of Surface Plasmon Resonance*, 2nd ed.; Schasfoort, R.B.M., Ed.; Royal Society of Chemistry: London, UK, 2017; ISBN 978-1-78262-730-2.
16. Homola, J. Surface Plasmon Resonance Sensors for Detection of Chemical and Biological Species. *Chem. Rev.* **2008**, *108*, 462–493. [CrossRef] [PubMed]
17. Hurot, C.; Brenet, S.; Buhot, A.; Barou, E.; Belloir, C.; Briand, L.; Hou, Y. Highly Sensitive Olfactory Biosensors for the Detection of Volatile Organic Compounds by Surface Plasmon Resonance Imaging. *Biosens. Bioelectron.* **2019**, *123*, 230–236. [CrossRef]
18. Pardoux, É.; Roux, A.; Mathey, R.; Boturyn, D.; Roupioz, Y. Antimicrobial Peptide Arrays for Wide Spectrum Sensing of Pathogenic Bacteria. *Talanta* **2019**, *203*, 322–327. [CrossRef]
19. Hyman, P. Phages for Phage Therapy: Isolation, Characterization, and Host Range Breadth. *Pharmaceuticals* **2019**, *12*, 35. [CrossRef]
20. O'Connell, L.; Roupioz, Y.; Marcoux, P. Optical Bacteriophage Susceptibility Testing by SPR (Surface Plasmon Resonance). In *Plasmonics in Biology and Medicine XVIII*; International Society for Optics and Photonics: Bellingham, WA, USA, 2021; Volume 11661, p. 116610O. [CrossRef]
21. O'Connell, L.; Marcoux, P.R.; Roupioz, Y. Strategies for Surface Immobilization of Whole Bacteriophages: A Review. *ACS Biomater. Sci. Eng.* **2021**, *7*, 1987–2014. [CrossRef]
22. Genuer, V.; Gal, O.; Méteau, J.; Marcoux, P.; Schultz, E.; Lacot, É.; Maurin, M.; Dinten, J.-M. Optical Elastic Scattering for Early Label-Free Identification of Clinical Pathogens. *Adv. Biomed. Clin. Diagnostic Surg. Guid. Syst. XIV* **2016**, *9698*, 96980A. [CrossRef]
23. Tardif, M.; Picard, E.; Gaude, V.; Jager, J.-B.; Peyrade, D.; Hadji, E.; Marcoux, P.R. On-Chip Optical Nano-Tweezers for Culture-Less Fast Bacterial Viability Assessment. *Small* **2022**, *18*, 2103765. [CrossRef]
24. Le Galudec, J.; Dupoy, M.; Rebuffel, V.; Marcoux, P.R. Mid-Infrared Multispectral Lensless Imaging for Wide-Field and Label-Free Microbial Identification. In *Biomedical Spectroscopy, Microscopy, and Imaging*; International Society for Optics and Photonics: Bellingham, WA, USA, 2020; Volume 11359. [CrossRef]
25. Marcoux, P.R.; Dupoy, M.; Cuer, A.; Kodja, J.L.; Lefebvre, A.; Licari, F.; Louvet, R.; Narassiguin, A.; Mallard, F. Optical Forward-Scattering for Identification of Bacteria within Microcolonies. *Appl. Microbiol. Biotechnol.* **2014**, *98*, 2243–2254. [CrossRef]
26. Tardif, M.; Jager, J.B.; Marcoux, P.R.; Uchiyamada, K.; Picard, E.; Hadji, E.; Peyrade, D. Single-Cell Bacterium Identification with a SOI Optical Microcavity. *Appl. Phys. Lett.* **2016**, *109*, 1–6. [CrossRef]
27. Rosenblum, E.D.; Tyrone, S. Serology, Density, and Morphology of Staphylococcal Phages. *J. Bacteriol.* **1964**, *88*, 1737–1742. [CrossRef] [PubMed]
28. Lee, L.F.; Boezi, J.A. Characterization of Bacteriophage Gh-1 for Pseudomonas Putida. *J. Bacteriol.* **1966**, *92*, 1821–1827. [CrossRef] [PubMed]
29. Adams, M.H. *Bacteriophages*; Interscience Publishers: New York, NY, USA, 1959.
30. Hosseinidoust, Z.; Olsson, A.L.J.; Tufenkji, N. Going Viral: Designing Bioactive Surfaces with Bacteriophage. *Colloids Surfaces B Biointerfaces* **2014**, *124*, 2–16. [CrossRef]
31. Tang, Z.; Huang, X.; Baxi, S.; Chambers, J.R.; Sabour, P.M.; Wang, Q. Whey Protein Improves Survival and Release Characteristics of Bacteriophage Felix O1 Encapsulated in Alginate Microspheres. *Food Res. Int.* **2013**, *52*, 460–466. [CrossRef]
32. Mandula, O.; Kleman, J.-P.; Lacroix, F.; Allier, C.; Fiole, D.; Hervé, L.; Blandin, P.; Kraemer, D.C.; Morales, S. Phase and Fluorescence Imaging with a Surprisingly Simple Microscope Based on Chromatic Aberration. *Opt. Express* **2020**, *28*, 2079. [CrossRef]
33. Tinevez, J.Y.; Perry, N.; Schindelin, J.; Hoopes, G.M.; Reynolds, G.D.; Laplantine, E.; Bednarek, S.Y.; Shorte, S.L.; Eliceiri, K.W. TrackMate: An Open and Extensible Platform for Single-Particle Tracking. *Methods* **2017**, *115*, 80–90. [CrossRef]
34. Rice, L.B. Federal Funding for the Study of Antimicrobial Resistance in Nosocomial Pathogens: No ESKAPE. *J. Infect. Dis.* **2008**, *197*, 1079–1081. [CrossRef]
35. Harwood, C.S.; Fosnaugh, K.; Dispensa, M. Flagellation of Pseudomonas Putida and Analysis of Its Motile Behavior. *J. Bacteriol.* **1989**, *171*, 4063–4066. [CrossRef]
36. Pollitt, E.J.G.; Diggle, S.P. Defining Motility in the Staphylococci. *Cell. Mol. Life Sci.* **2017**, *74*, 2943–2958. [CrossRef]
37. O'Connell, L.; Roupioz, Y.; Marcoux, P.R. Container Material Dictates Stability of Bacteriophage Suspensions: Light Scattering & Infectivity Measurements Reveal Mechanisms of Infectious Titer Decay. *J. Appl. Microbiol.* **2022**, 1–15. [CrossRef]
38. Richter, Ł.; Księżarczyk, K.; Paszkowska, K.; Janczuk-Richter, M.; Niedziółka-Jönsson, J.; Gapiński, J.; Łoś, M.; Hołyst, R.; Paczesny, J. Adsorption of Bacteriophages on Polypropylene Labware Affects Reproducibility of Phage Research. *Sci. Rep.* **2021**, *11*, 7387. [CrossRef] [PubMed]
39. Kovalyova, I.V.; Kropinski, A.M. The Complete Genomic Sequence of Lytic Bacteriophage Gh-1 Infecting Pseudomonas Putida—Evidence for Close Relationship to the T7 Group. *Virology* **2003**, *311*, 305–315. [CrossRef]
40. Li, X.; Gerlach, D.; Du, X.; Larsen, J.; Stegger, M.; Kuhner, P.; Peschel, A.; Xia, G.; Winstel, V. An Accessory Wall Teichoic Acid Glycosyltransferase Protects Staphylococcus Aureus from the Lytic Activity of Podoviridae. *Sci. Rep.* **2015**, *5*, 1–10. [CrossRef] [PubMed]
41. Rajaure, M.; Berry, J.; Kongari, R.; Cahill, J.; Young, R. Membrane Fusion during Phage Lysis. *Proc. Natl. Acad. Sci. USA* **2015**, *112*, 5497–5502. [CrossRef]

42. Bradley, D.E. Spheroplast Formation in Cells of Escherichia Coli Infected with a Phi-X 174 Type Bacteriophage. *J. Gen. Virol.* **1968**, *3*, 141–142. [CrossRef]
43. World Health Organization. *Antimicrobial Resistance Global Report on Surveillance*; World Health Organization: Geneva, Switzerland, 2014.